Supporting Information

Fabrication of SnS_2/Mn_2SnS_4/Carbon Heterostructures for Sodium-Ion Batteries with High Initial Coulombic Efficiency and Cycling Stability

Xing Ou,[a,§] Liang Cao,[a,§] Xinghui Liang,[a] Fenghua Zheng,[a] Hong-Sheng Zheng,[b] Xianfeng Yang,[c] Jeng-Han Wang,[b] Chenghao Yang,[a,*] Meilin Liu[a,d]

[a] *Guangzhou Key Laboratory for Surface Chemistry of Energy Materials, New Energy Research Institute, School of Environment and Energy, South China University of Technology, Guangzhou 510006, P. R. China*

[b] *Department of Chemistry, National Taiwan Normal University, Taipei, 11677, Taiwan*

[c] *Analytical and Testing Center, South China University of Technology, Guangzhou, 510641 P. R. China*

[d] *School of Materials Science & Engineering, Georgia Institute of Technology, Atlanta, GA30332-0245, USA*

[*] Corresponding author. E-mail: esyangc@scut.edu.cn (C. Yang).

[§] These authors contributed equally.

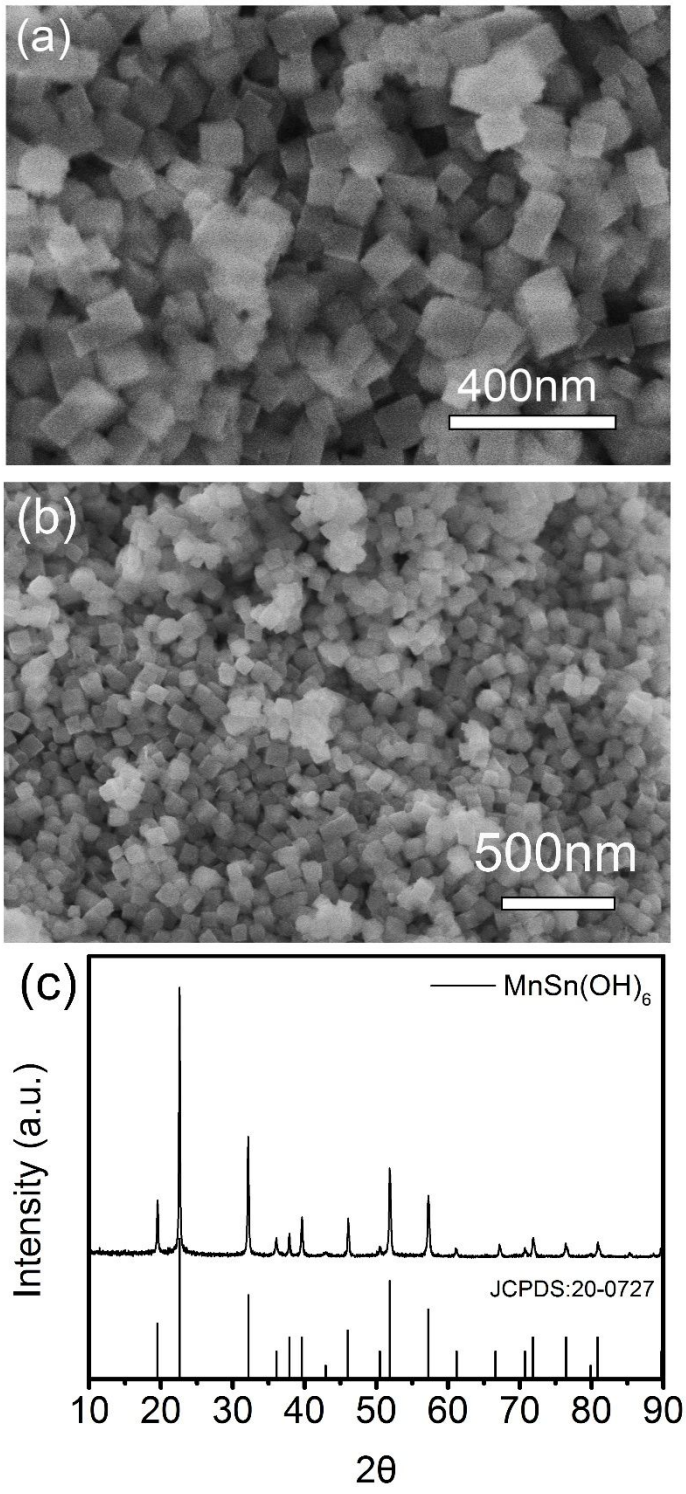

Figure S1. (a,b) SEM image and (c) XRD pattern of $MnSn(OH)_6$ precursors.

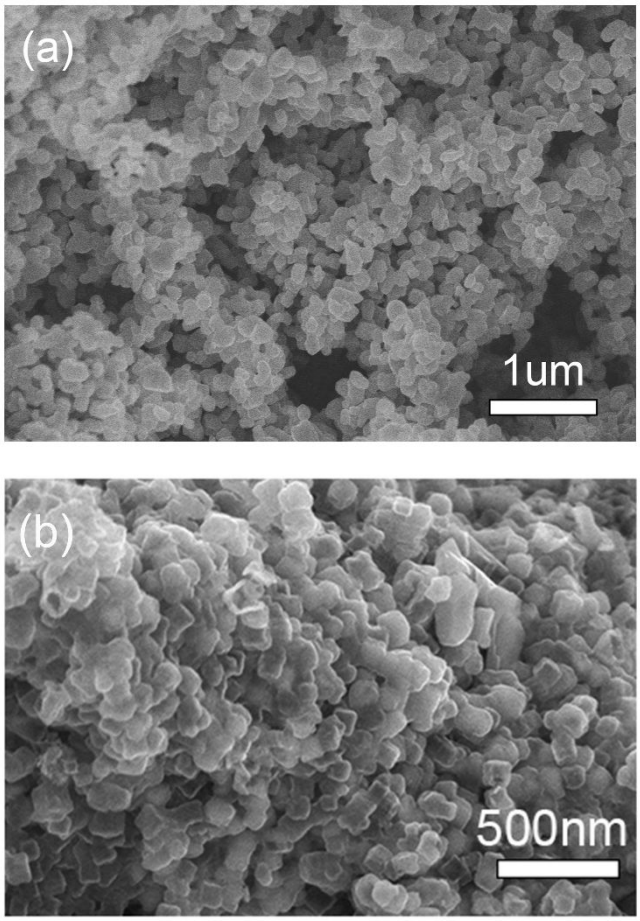

Figure S2. (a,b) SEM images of SMS nanoboxes.

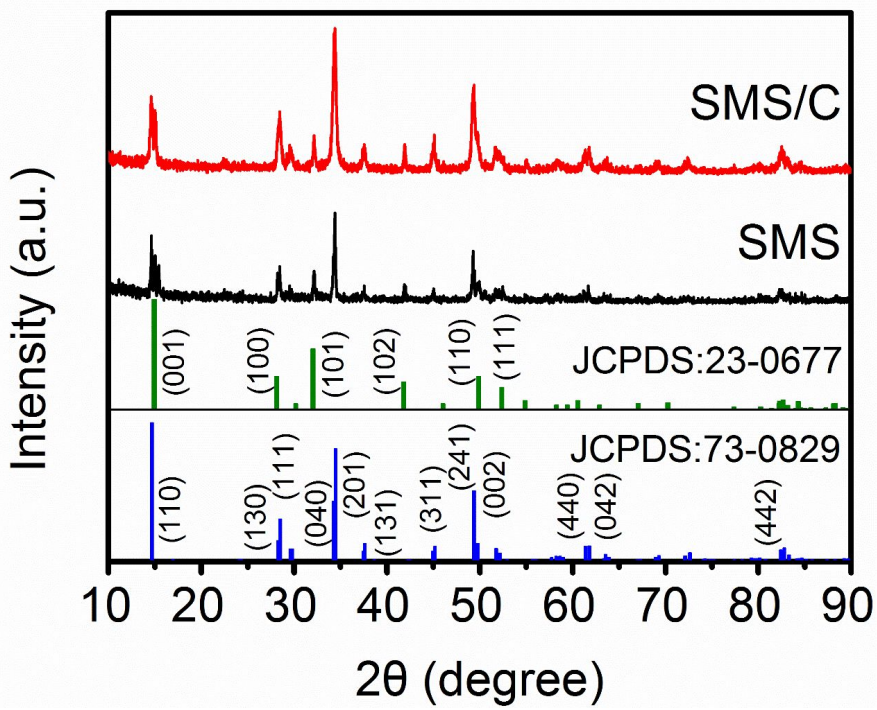

Figure S3. XRD patterns of SMS and SMS/C.

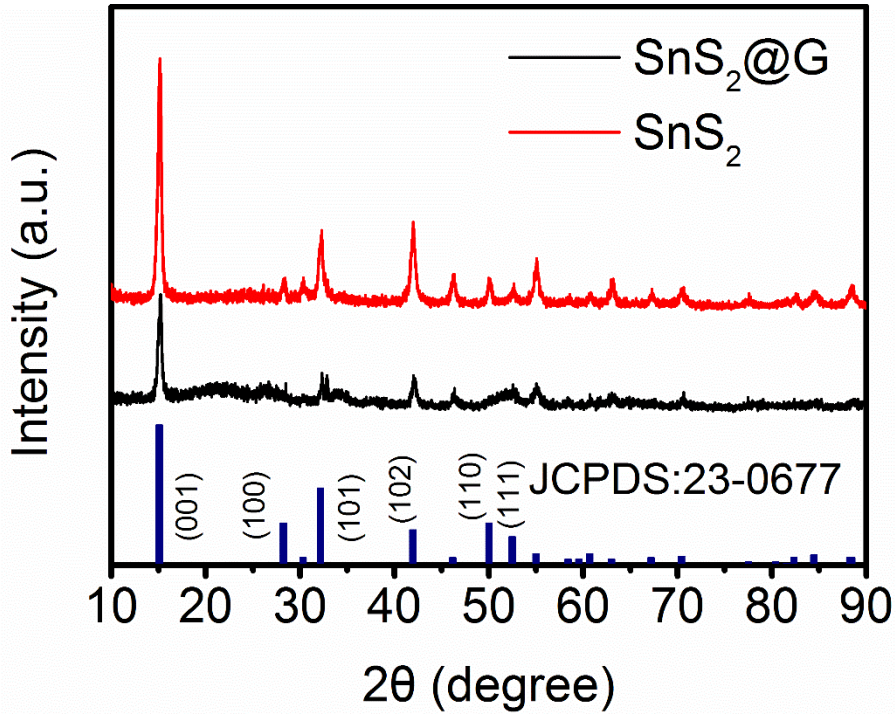

Figure S4. XRD patterns of SnS_2 and SnS_2/C.

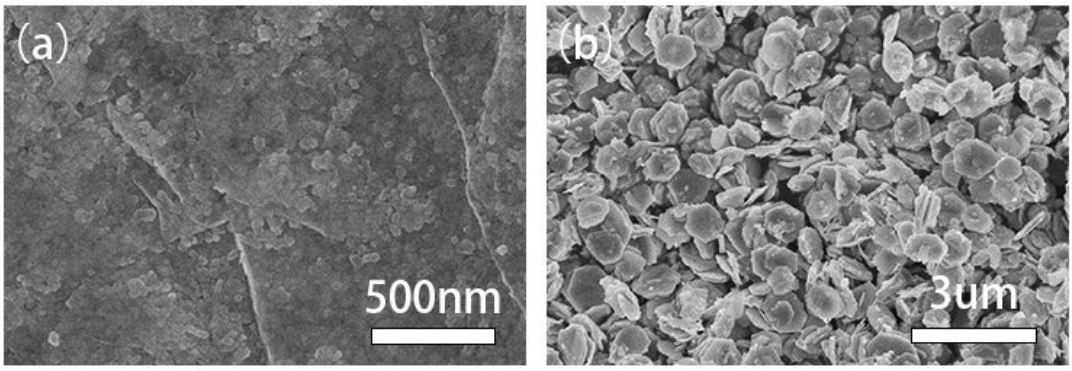

Figure S5. SEM images of (a) SnS_2/C and (b) SnS_2.

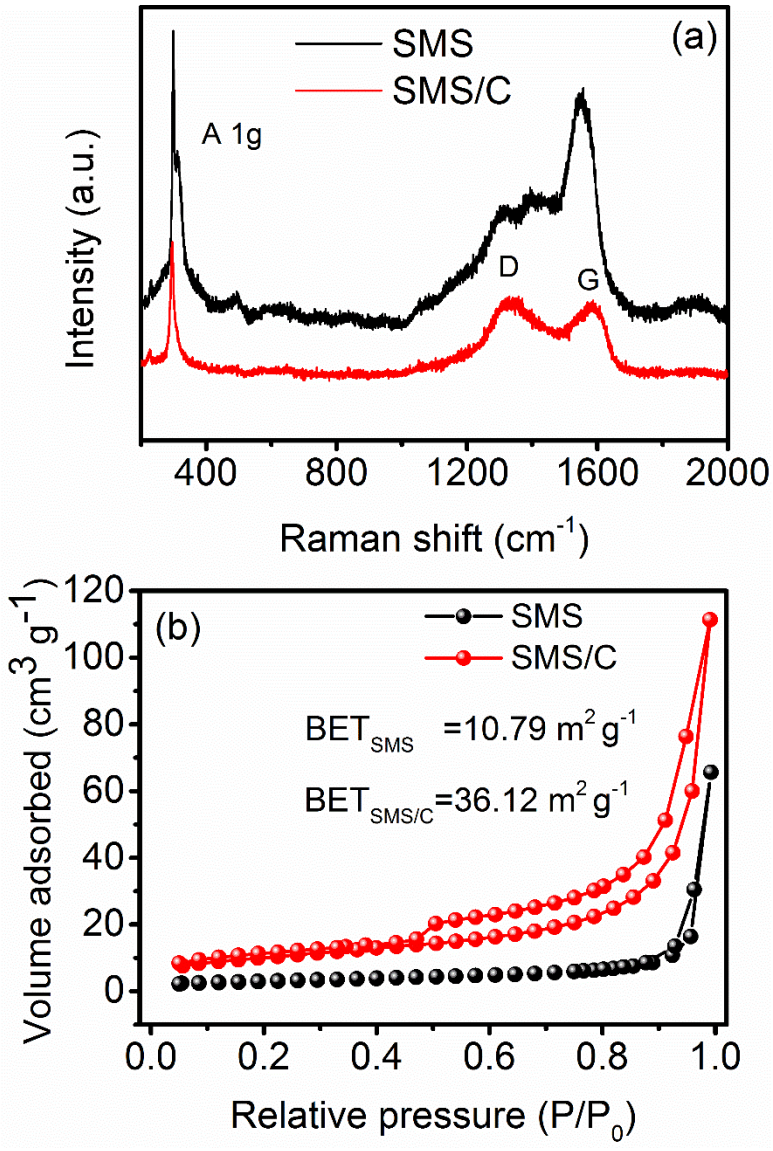

Figure S6. (a) Raman spectra and (b) BET results of SMS and SMS/C.

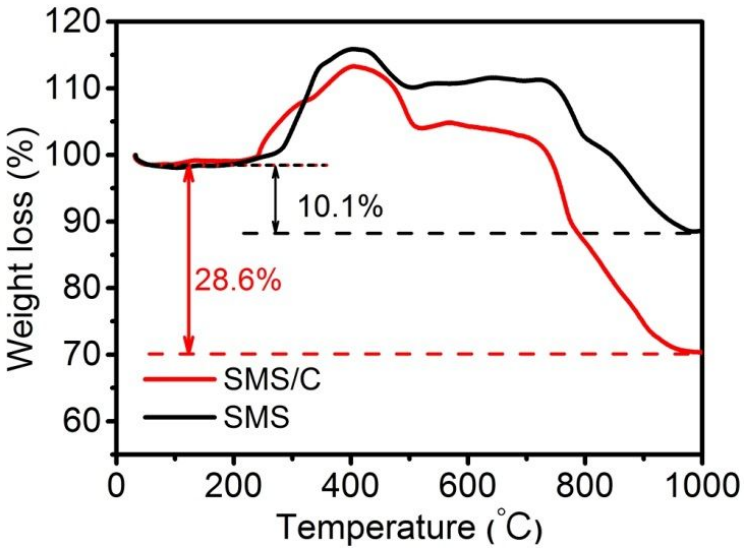

Figure S7. TGA results of SMS and SMS/C composites.

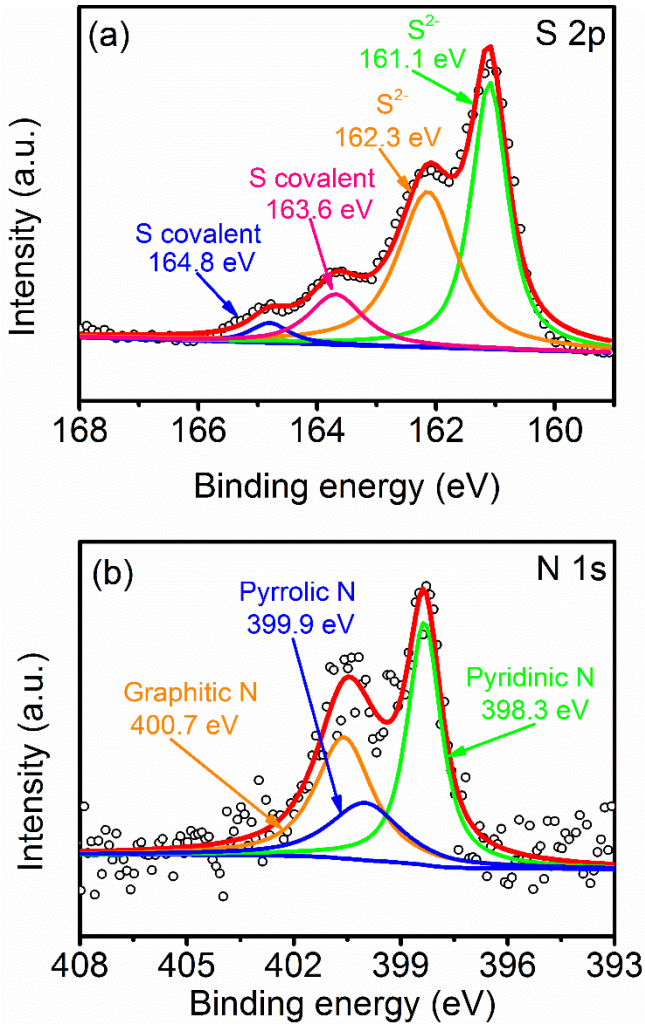

Figure S8. The XPS results of (a) S 2p and (b) N 1s spectrum of SMS/C.

Table S1. The comparison of ICEs and cycling performance among the Sn-based sulfide materials for SIBs anodes.

Sample	Cycle number	Current density ($mA\ g^{-1}$)	Capacity retention (%)	Initial coulombic efficicency (%)	reference
SnS_2@Aerogel graphene	100	50	68	53.4	S1
SnS_2- rGO	1000	800	62.5	64	S2
SnS_2@N- rGO	200	500	86.7	66.5	S3
SnS_2@ rGO	100	200	81	81	S4
C@SnS_2@C	1000	5000	90.2	56	S5
MoS_2/SnS_2@rGO	200	750	87.2	84.2	S6
SnS_2 nanosheet	300	1000	89.2	72	S7
SnS_2@ hollow C	100	200	87.6	74.3	S8
SnS_2@CoS_2-rGO	100	200	76	86	S9
SnS_2 nanowall	100	500	85	75.2	S10
SMS/C	500	5000	91.3	90.8	This work

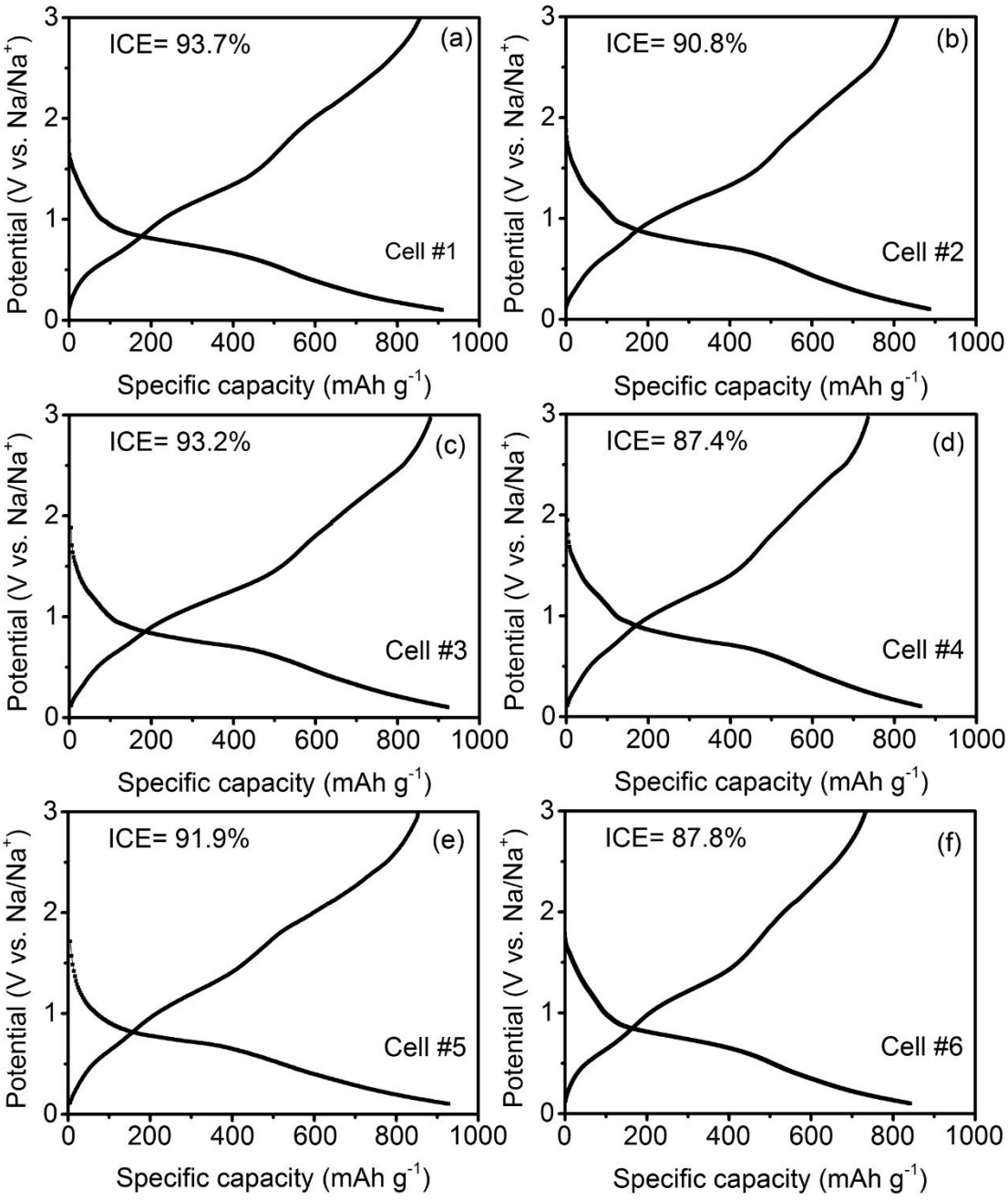

Figure S9. ICE of SMS/C electrodes with six different batteries.

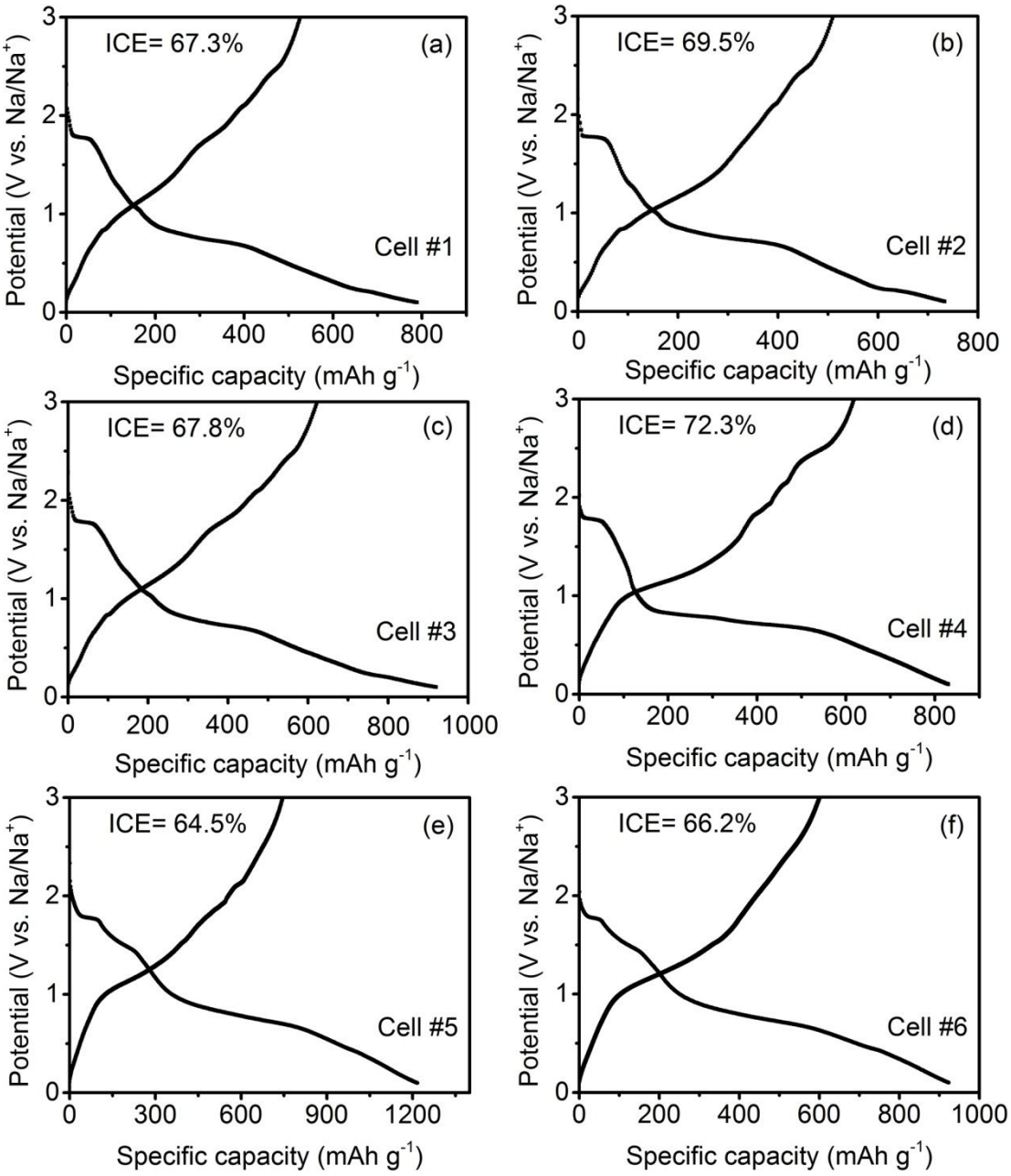

Figure S10. ICE of SnS_2 electrodes with six different batteries.

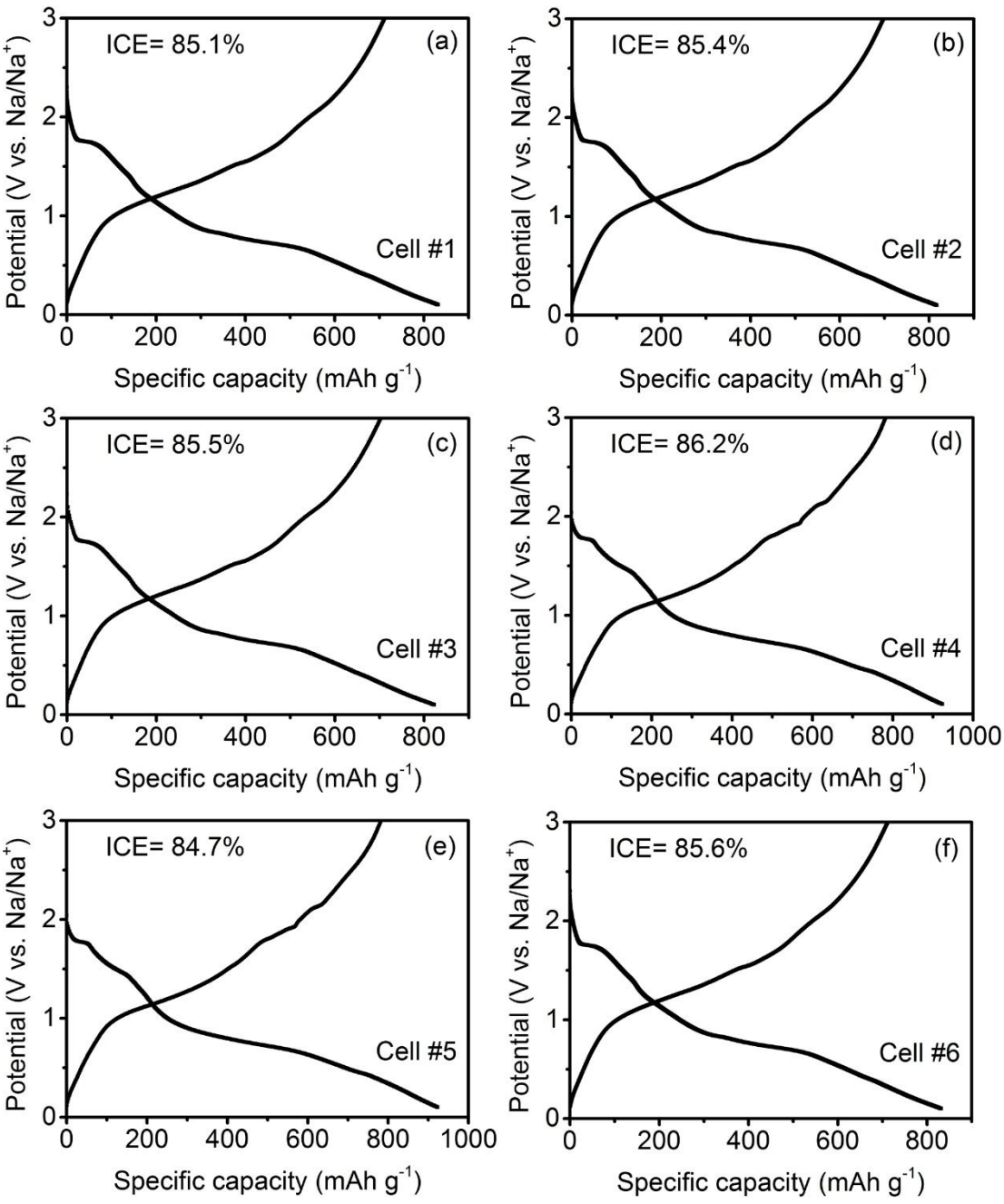

Figure S11. ICE of SnS_2/C electrodes with six different batteries.

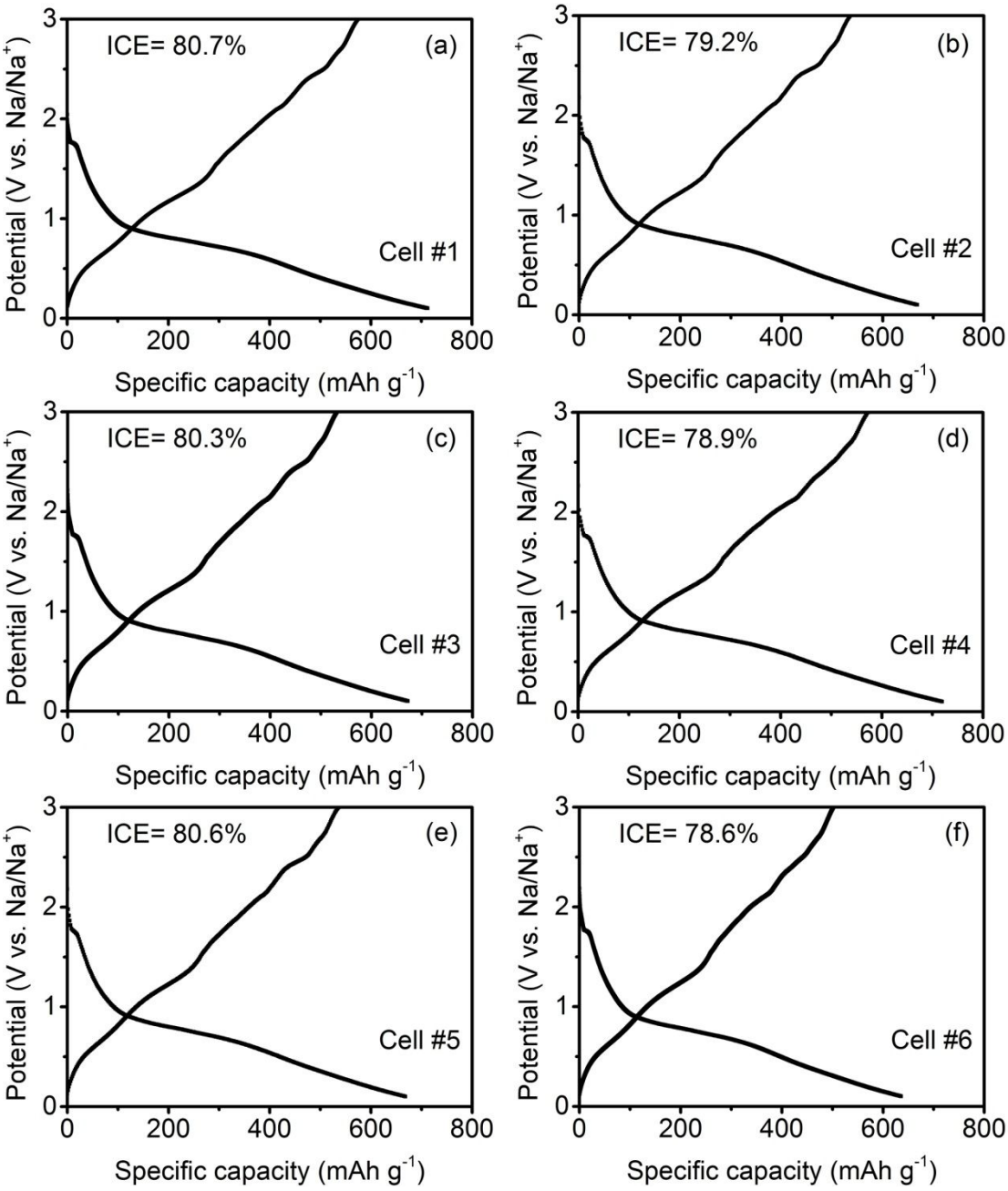

Figure S12. ICE of SMS electrodes with six different batteries.

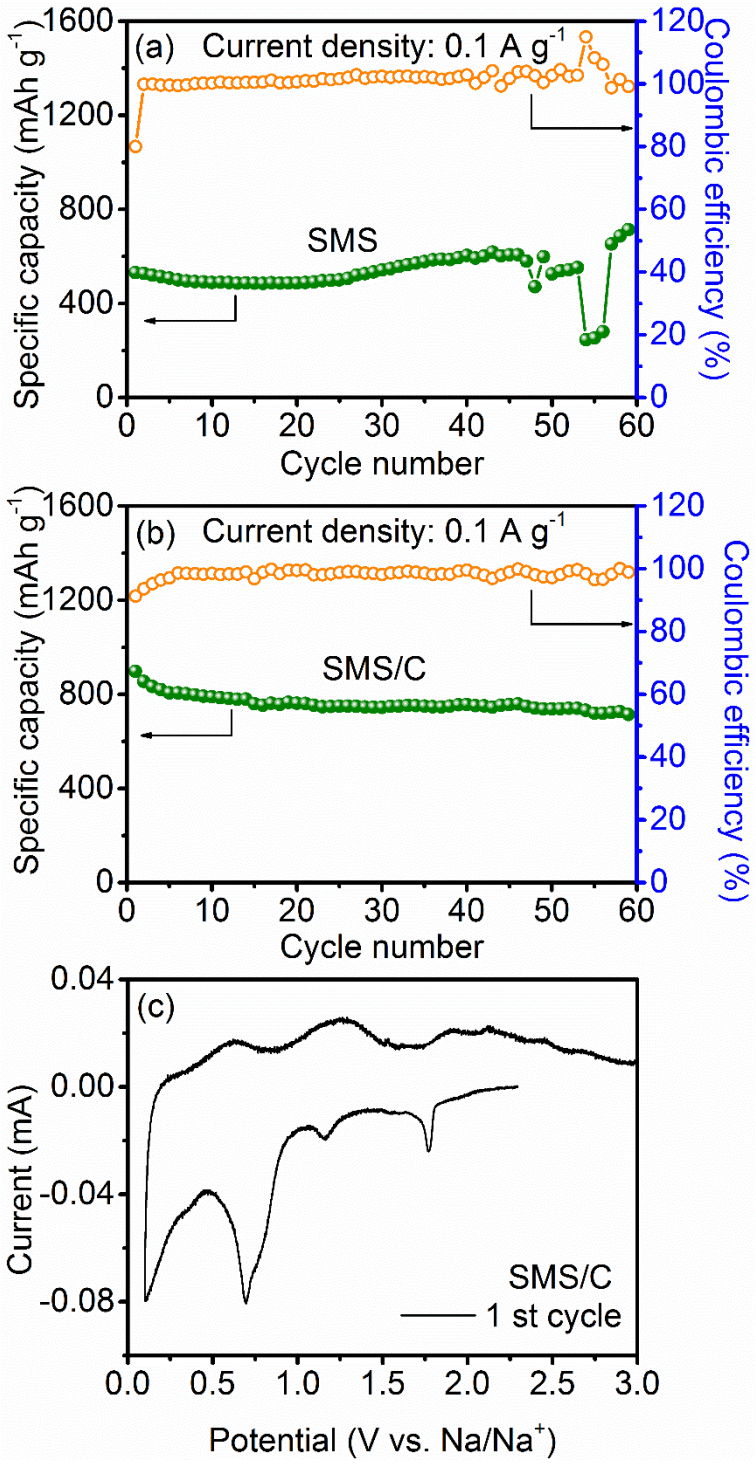

Figure S13. The cycling performance of (a) SMS and (b) SMS/C electrodes at 0.1 A g^{-1}. (c) CV curve at initial cycle for SMS/C electrode

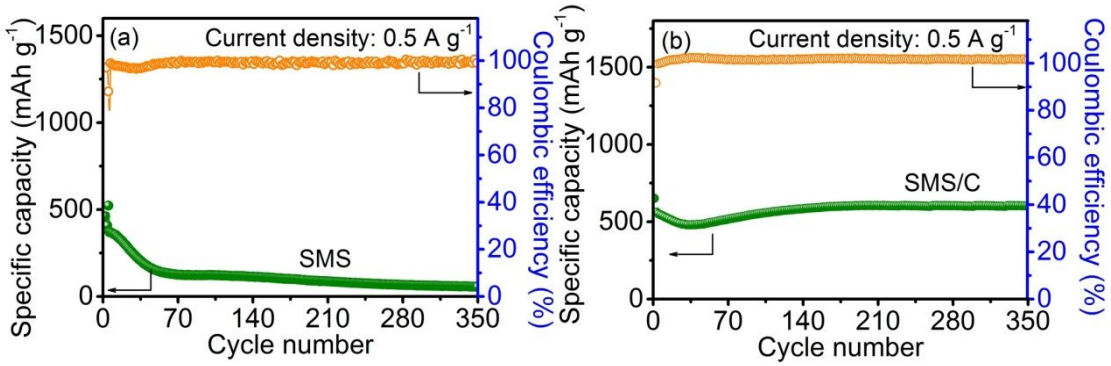

Figure S14. The cycling performance of (a) SMS and (b) SMS/C electrodes at 0.5 A g^{-1}.

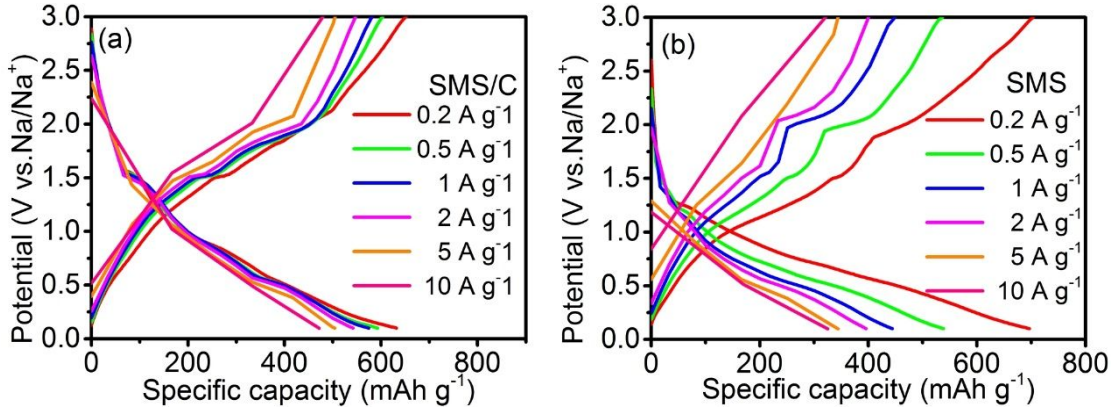

Figure S15. The charge-discharge curves of (a) SMS/C and (b) SMS electrodes at different current density.

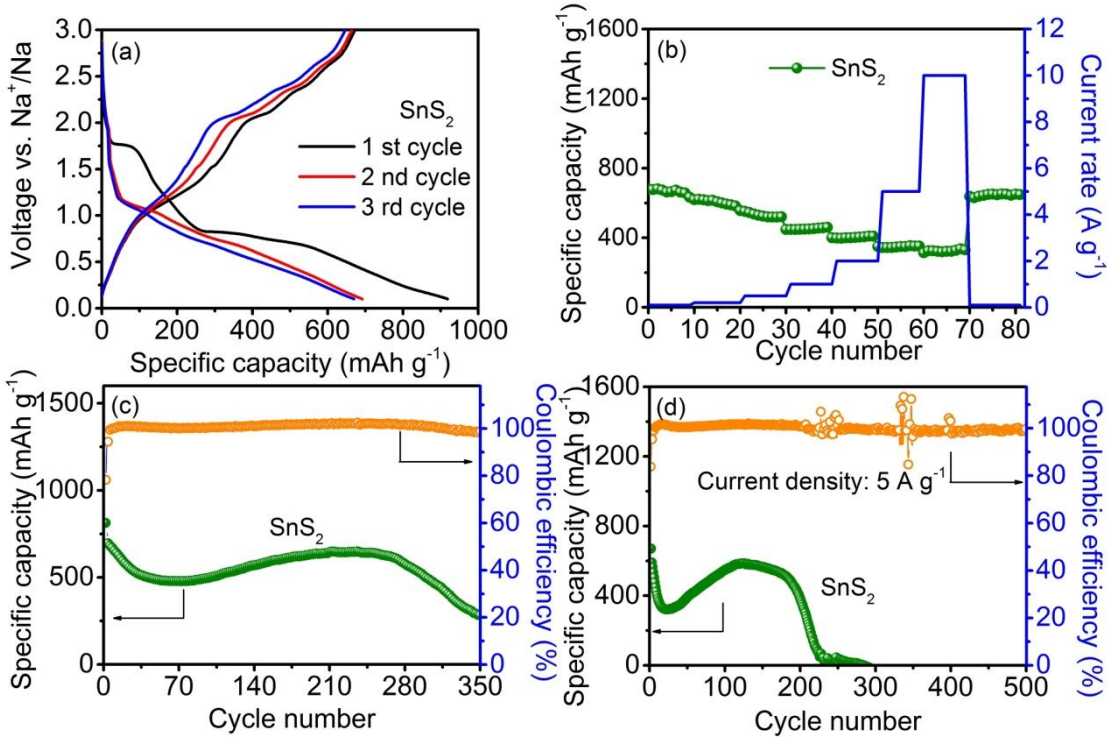

Figure S16. Electrochemical performance of SnS_2 electrodes: (a) First three cycle charge-discharge curves, (b) rate performance, cycling performance at rate of (c) 0.5 A g^{-1} and (d) 5 A g^{-1}.

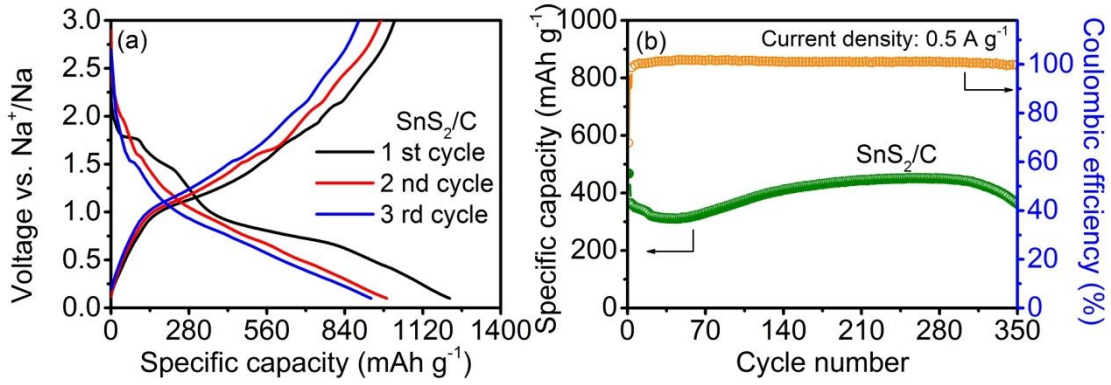

Figure S17. (a) First three charge-discharge curves of SnS_2/C electrode. (b) Cycling performance of SnS_2/C electrode at 0.5 A g^{-1}.

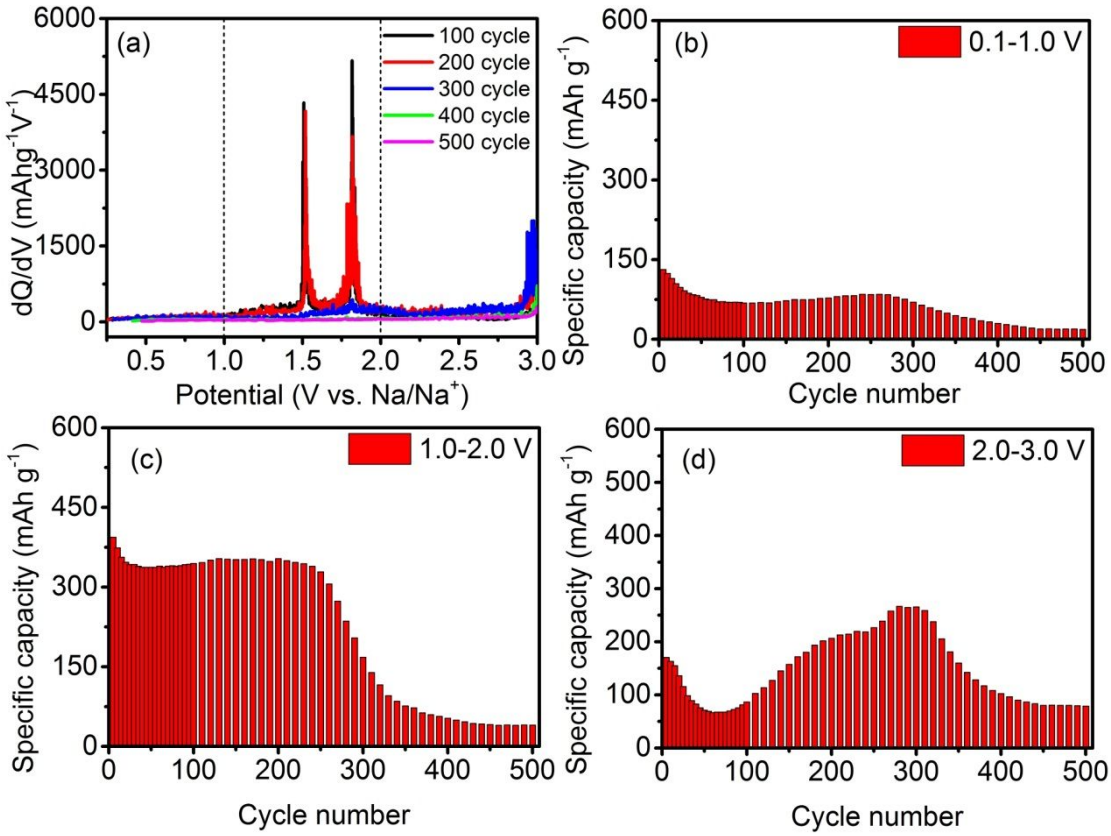

Figure S18. (a) The differential charge capacity curves *versus* voltage at the various cycles for the SnS_2/C composite in 0.1-3.0 V at rate of 0.5 A g^{-1}. Reversible capacities versus cycle number of SnS_2/C composite separated into potential ranges of (b) 0.1-1.0 V, (c) 1.0-2.0 V, and (d) 2.0-3.0 V.

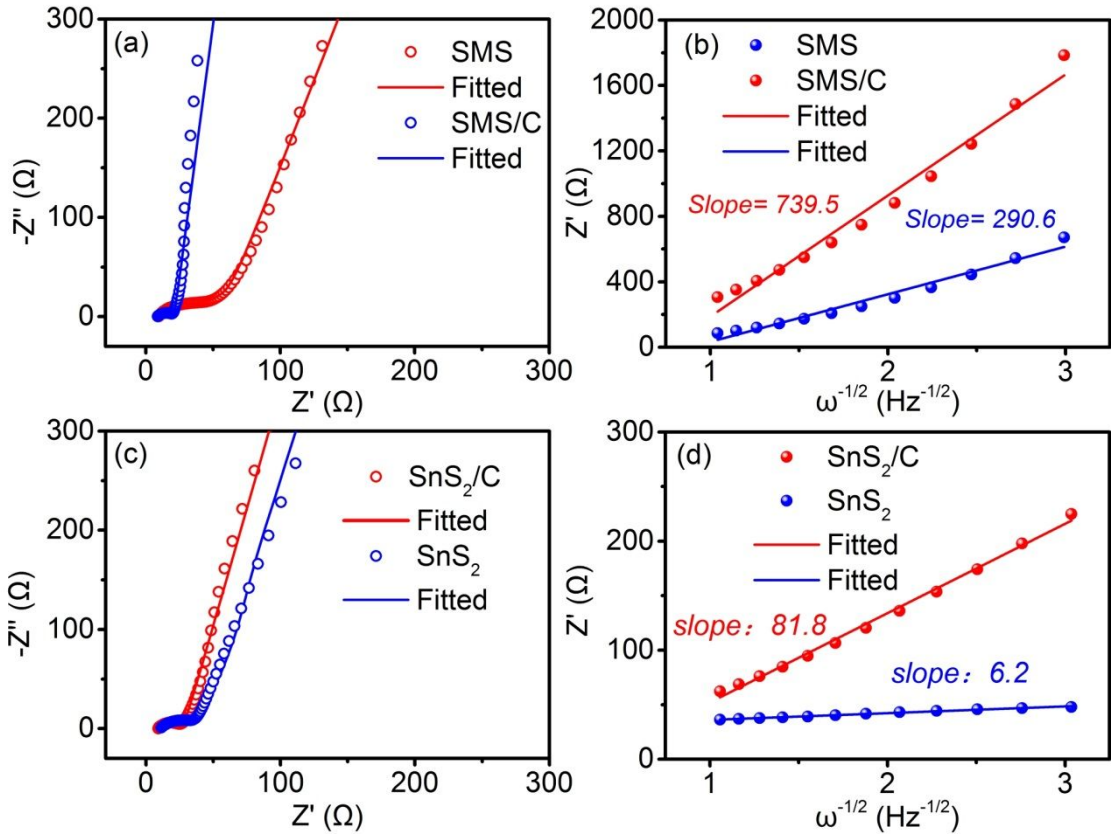

Figure S19. EIS measurement and the relationship plot of Z' versus $\omega^{-1/2}$ at low-frequency region for SMS and SMS/C (a,b), SnS_2 and SnS_2/C (c, d).

Equation S1:

$$D_{Na^+} = \frac{R^2T^2}{2n^4F^4A^2C^2\sigma_w^2} \quad \text{(S1)}$$

Equation S2:

$$Z' = R_\Omega + R_{ct}\sigma_w^{-1/2} \quad \text{(S2)}$$

Where *R, T, F, n, A, C* and σ_w are the gas constant, the absolute temperature, the surface area of the electrode, the Faraday's constant, the number of electrons per molecule during oxide, the insertion/extraction Na^+ concentration in the anode material and the Warburg factor, respectively.

Table S2. Fitting result of EIS in Figure S20 with the equivalent circuit proposed.

Samples	R_s(Ω)	R_{ct}(Ω)	σ (Ω cm^2 s$^{-1/2}$)	D_{Na^+}(cm^2 s^{-1})
SMS	8.731	56.26	739.5	9.28×10^{-16}
SMS/C	8.645	12.33	290.6	6.01×10^{-15}
SnS_2	8.756	19.41	6.2	1.65×10^{-17}
SnS_2/C	10.7	27.21	81.8	2.87×10^{-15}

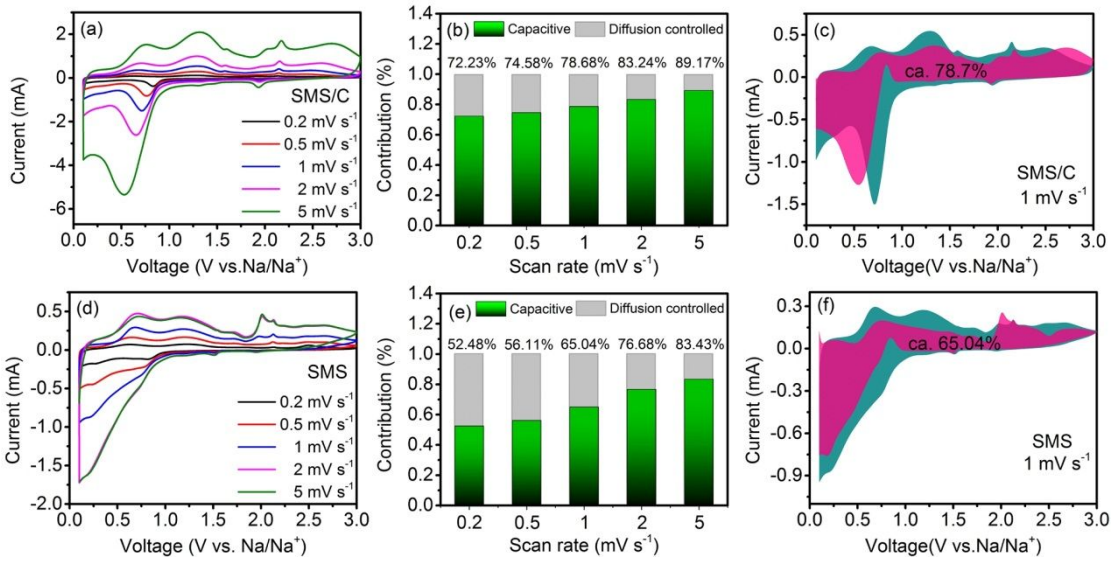

Figure S20. (a,c) The CV curves of SMS/C and SMS electrodes at different scan rates from 0.2 to 5 mV s^{-1}. (b,d) The capacity contribution of SMS/C and SMS electrodes at different scan rates. (c,f) The capacity contribution of SMS/C and SMS at a specific scan rate of 1 mV s^{-1}.

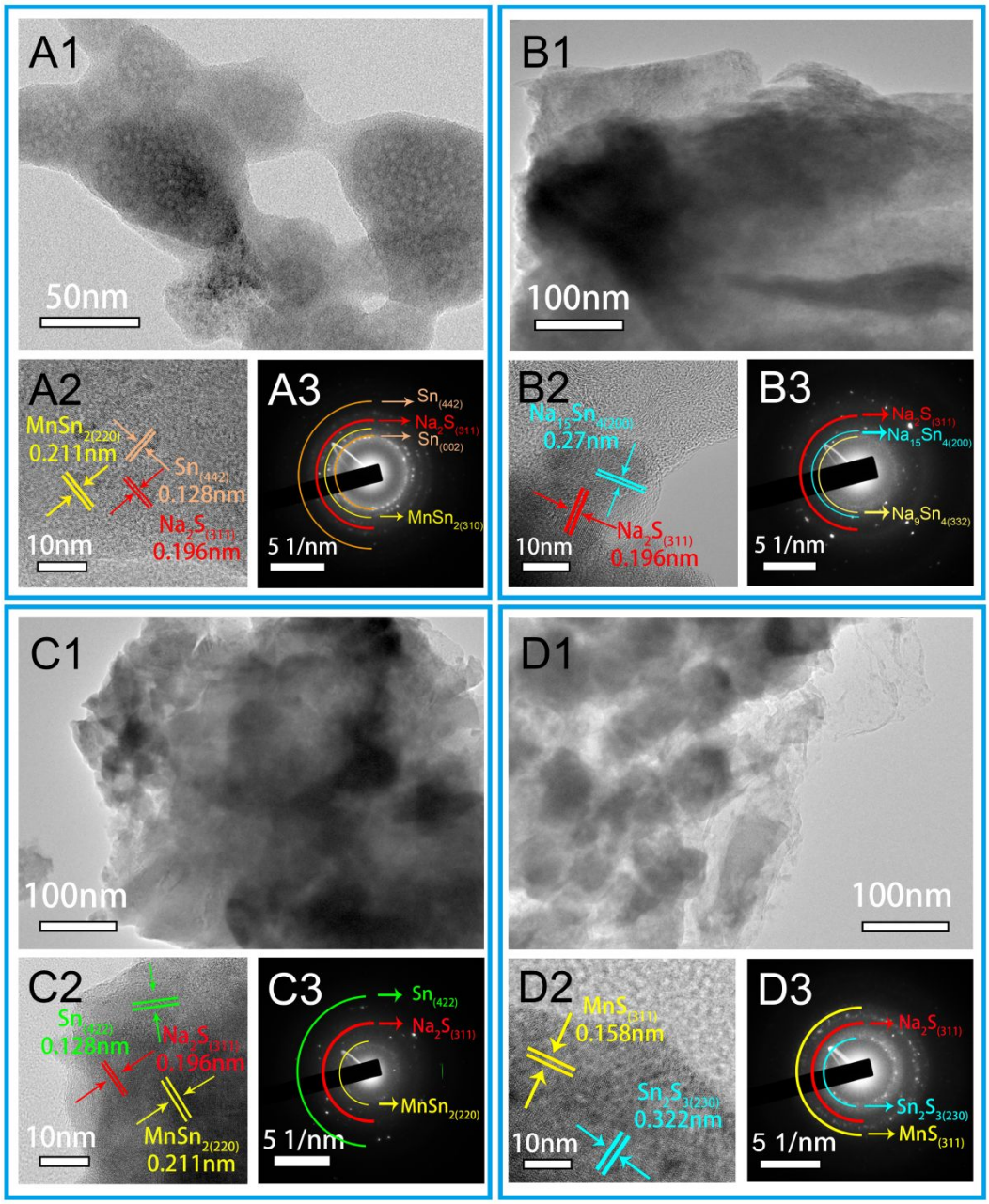

Figure S21. *Ex-situ* TEM results of SMS/C electrode at different charge-discharge states (A1-A3, 0.8 V; B1-B3, 0.1 V; C1-C3, 1.5 V; D1-D3, 3.0 V).

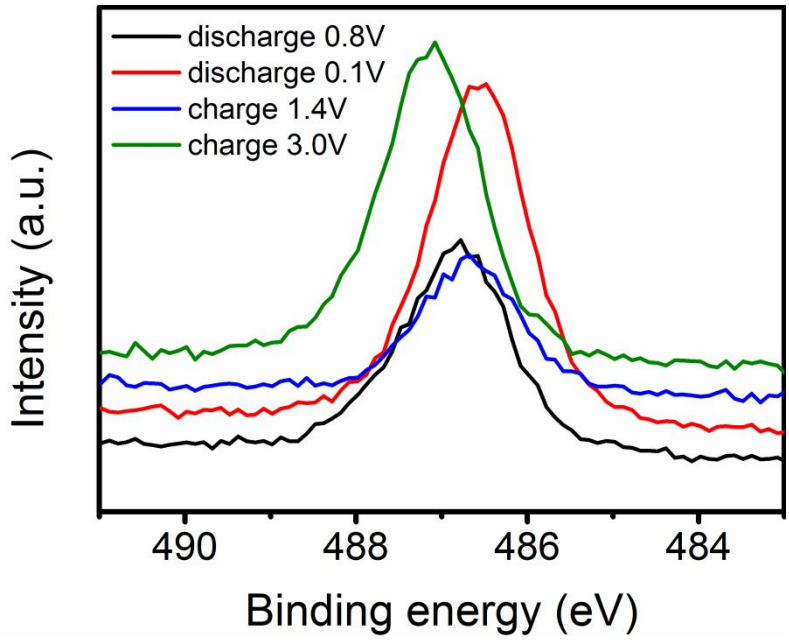

Figure S22. *Ex-situ* XPS measurement of SMS/C electrode at different charge-discharge states.

According to the ex-situ XPS results, the peak of Sn $3d_{5/2}$ of SMS/C electrode shifts to lower binding position during the discharge process, indicating the reduction reaction from Sn^{4+} to metallic Sn^0. In the coresponding charge process, the peak of Sn $3d_{5/2}$ reture back to the high binding position, which closes to the prinsite state, suggesting the highly reversibility for the conversion reaction from Sn^0 to Sn-S-Mn sulfide.

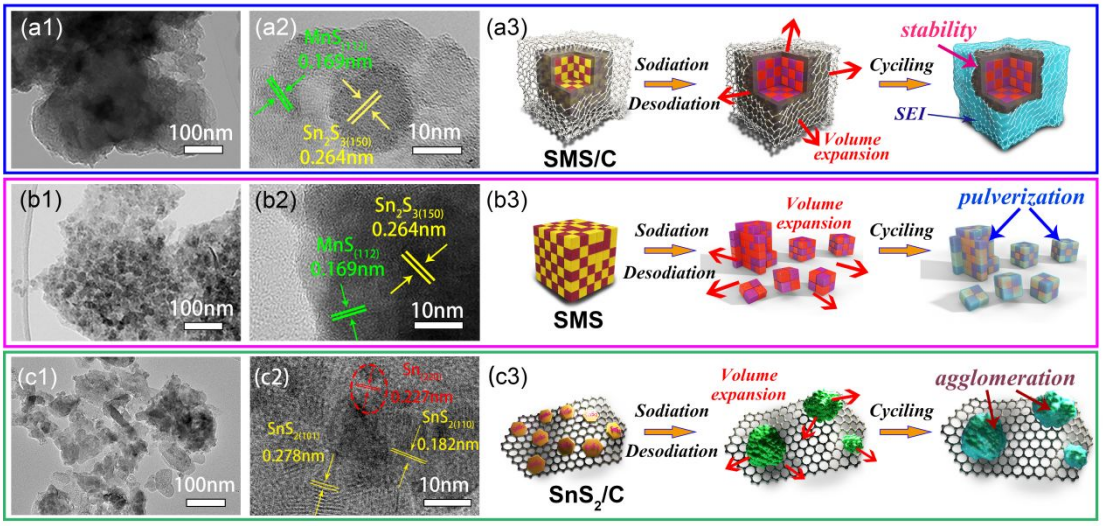

Figure S23. *Ex-situ* TEM and HRTEM images, and schematic illustration during long-term cycling for the (a) SMS/C, (b) pristine SMS and (c) SnS_2/C electrodes after 100 cycles.

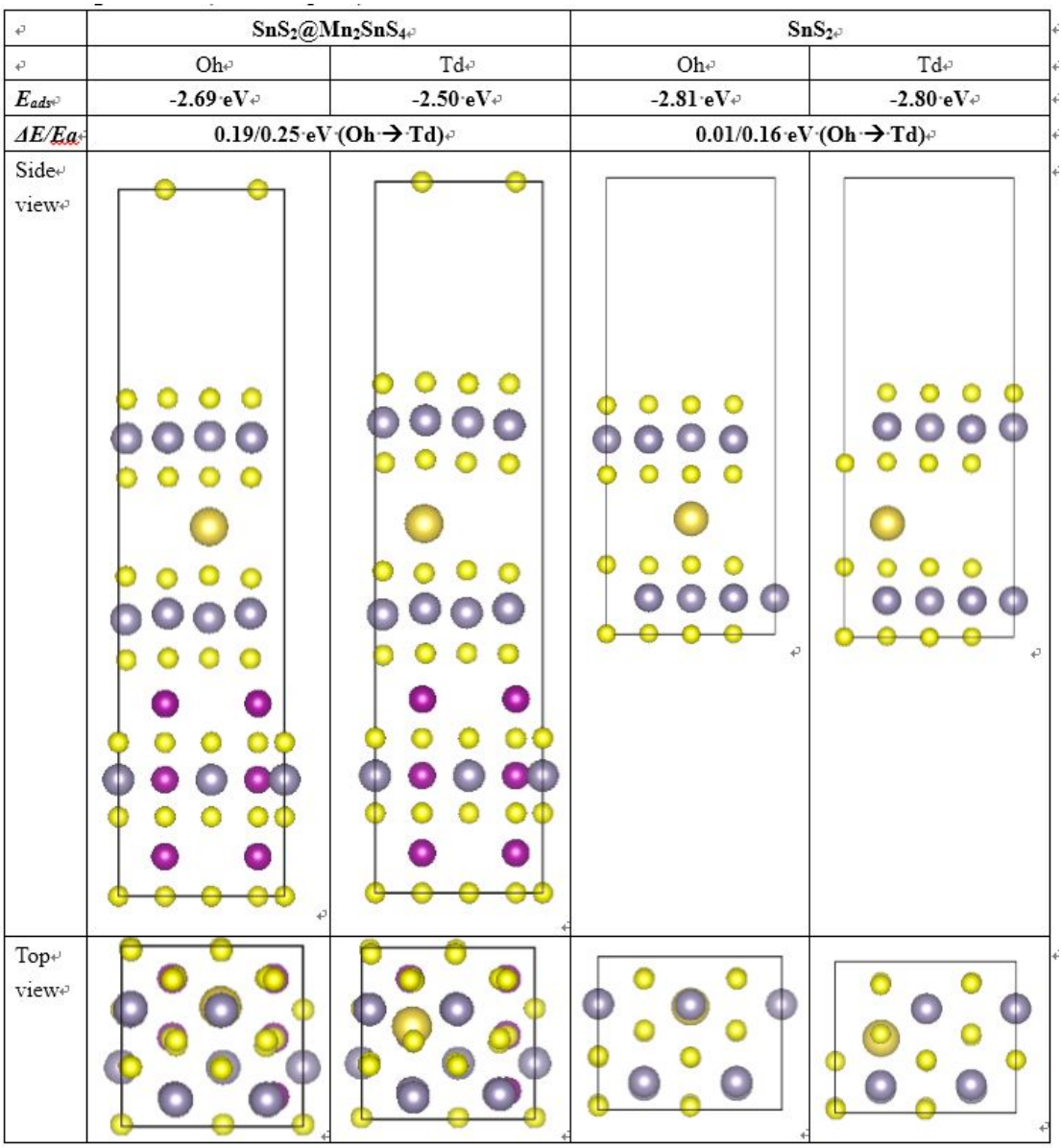

Figure S24. Energetic result of Na^+ adsorption (E_{ads}, ΔE and Ea) for SnS_2@Mn_2SnS_4 and pure SnS_2. (Na^+: large yellow sphere. Sn: grey; sphere. S: small yellow sphere. Mn: purple sphere).

	SnS_2		$SnS_2@Mn_2SnS_4$	
	Na^+ in **Oh**	Na^+ in **Td**	Na^+ in **Oh**	Na^+ in **Td**
Side view 1	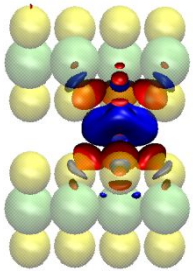	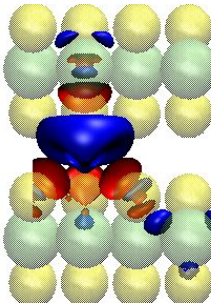	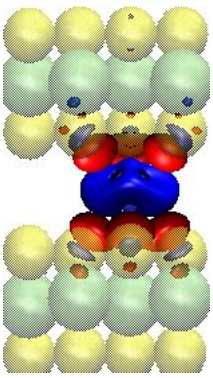	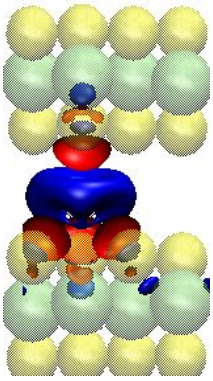
Side view 2	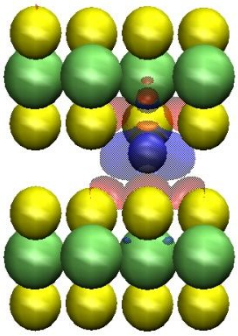	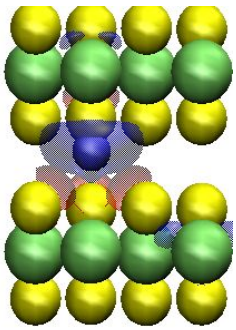	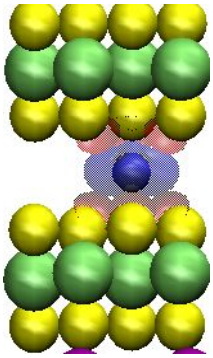	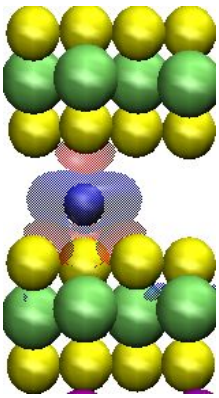
Top view	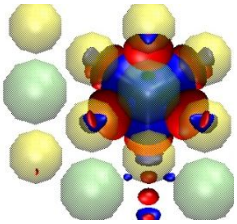	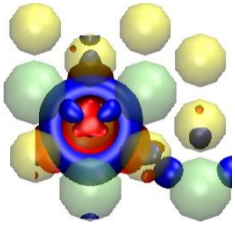	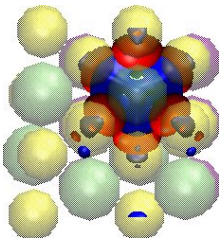	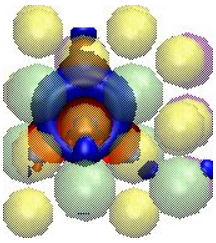
Botto m view	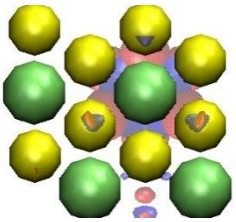	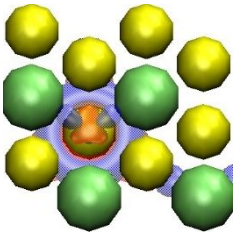	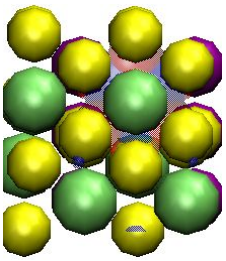	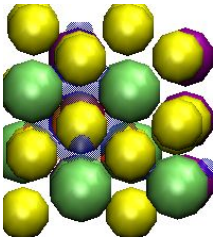

Figure S25. Charge density analysis of $SnS_2@Mn_2SnS_4$ and pure SnS_2.

Both SnS_2 and Mn_2SnS_4 shows similar charge density distribution that shows Na^+ with six bonds (each 3 in top and bottom) in Oh site and four bonds in Td site and explains the similar adsorption energies of them.

	$SnS_2@Mn_2SnS_4$		SnS_2	
	Oh	Td	Oh	Td
E_{ads}	-1.40 eV	-1.66 eV	-2.21 eV	-2.07 eV
Side view	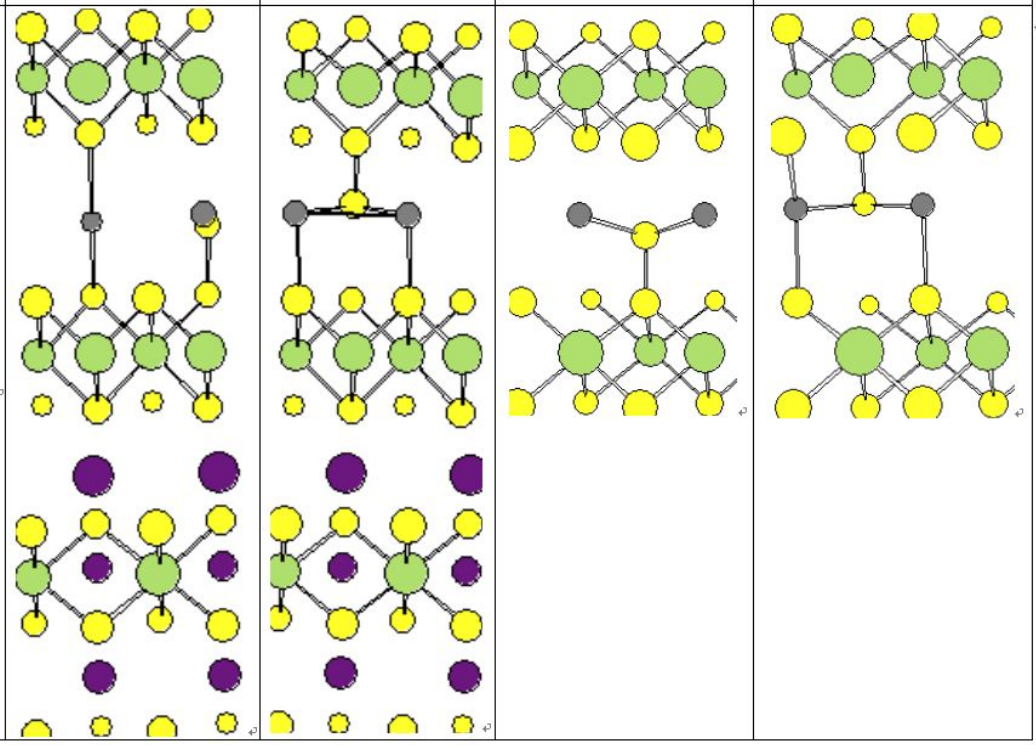			

Figure S26. Na_2S adsorption in the tunnel for $SnS_2@Mn_2SnS_4$ and pure SnS_2.

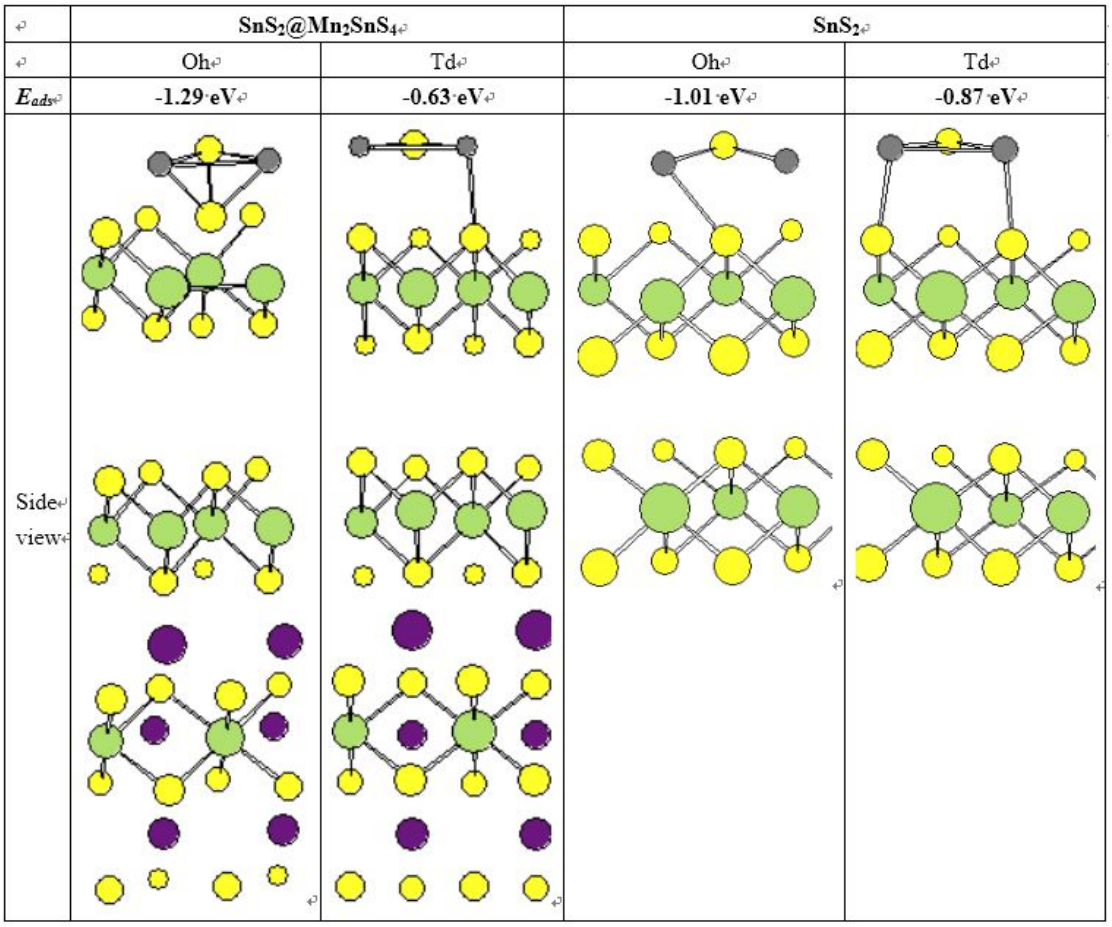

Figure S27. Na_2S adsorption on the surface for $SnS_2@Mn_2SnS_4$ and pure SnS_2.

Table S3. Coordinate change for Na^+ adsorption in the tunnel.

	$SnS_2@Mn_2SnS_4$		**SnS_2**	
	Oh	Td	Oh	Td
Coordinate change in **x**	0.01	0.01	0.01	-0.01
Coordinate change in **y**	-0.05	-0.13	0.10	0.02
Coordinate change in **z**	0.55	0.58	3.77	1.55

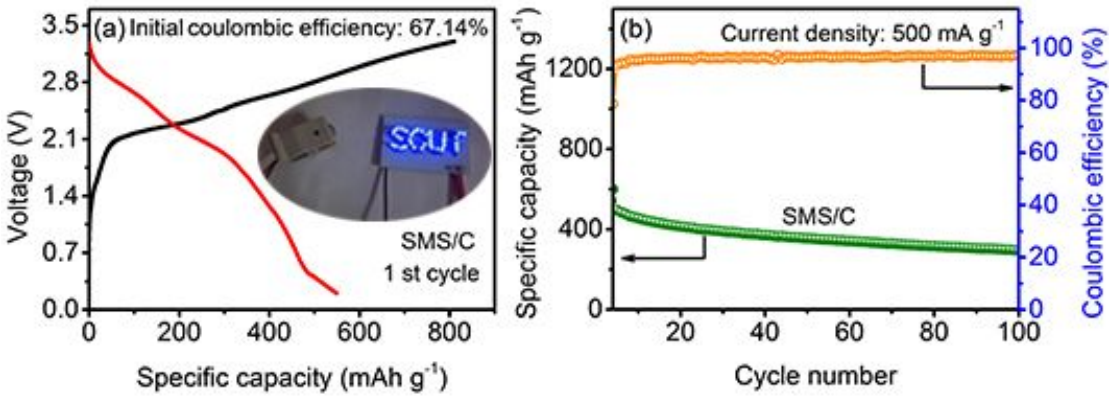

Figure S28. The full cell performances of SMS/C electrode. ($Na_3V_2(PO_4)_3$ active material as counter electrode)

Based on the aforementioned results, the full cells with self-synthesized $Na_3V_2(PO_4)_3$ (NVP) as the cathode were assembled, whose electrochemical property was presented in Figure S28a, further verifying the performance of SMS/C composite. The initial charge and discharge capacities are about 810.5 and 544.2 mAh g^{-1}, respectively, with an initial coulombic efficiency of 67.14%. In addition, after 100 cycles at a current density of 500 mA g^{-1}, the full cell of SMS/C can deliver a reverse capacity of 295 mAh g^{-1}, as shown in Figure S28b. Compared with the excellent initial coulombic efficiency of SMS/C half cell, the initial coulombic efficiency of SMS/C full cell is relative lower, which may attribute to the irreversible electrochemical reactions. Moreover, the electrolyte of full cell is not matched well with the both cathode and anode, causing a relative higher consume of Na^+ in formation of SEI on the both surface of anode and cathode.[S11,S12]

Reference

(S1) Fan, L.; Li, X.; Song, X.; Hu, N.; Xiong, D.; Koo, A.; Sun, X. Promising Dual-Doped Graphene Aerogel/SnS_2 Nanocrystal Building High Performance Sodium Ion Batteries. *ACS Appl. Mater. Interfaces* **2018**, *10*, 2637-2648.

(S2) Tao, S.; Wu, D.; Chen, S.; Qian, B.; Chu, W.; Song, L. A Versatile Strategy for Ultrathin SnS_2 Nanosheets Confined in a N-Doped Graphene Sheet Composite for High Performance Lithium and Sodium-Ion Batteries. *Chem. Commun.* **2018,** *54*, 8379-8382.

(S3) Qu, B.; Ma, C.; Ji, G.; Xu, C.; Xu, J.; Meng, Y. S.; Wang, T.; Lee, J. Y. Layered SnS_2-Reduced Graphene Oxide Composite-a High-Capacity, High-Rate, and Long-Cycle Life Sodium-Ion Battery Anode Material. *Adv. mater.* **2014,** *26*, 3854-3859.

(S4) Zhang, Y.; Zhu, P.; Huang, L.; Xie, J.; Zhang, S.; Cao, G.; Zhao, X. Few-Layered SnS_2 on Few-Layered Reduced Graphene Oxide as Na-Ion Battery Anode with Ultralong Cycle Life and Superior Rate Capability. *Adv. Funct. Mater.* **2015,** *25*, 481-489.

(S5) Qin, J.; Zhao, N.; Shi, C.; Liu, E.; He, F.; Ma, L.; Li, Q.; Li, J.; He, C. Sandwiched C@SnO_2@C Hollow Nanostructures as an Ultralong-Lifespan High-Rate Anode Material for Lithium-Ion and Sodium-Ion Batteries. *J. Mater. Chem. A* **2017,** *5*, 10946-10956.

(S6) Jiang, Y.; Guo, Y.; Lu, W.; Feng, Z.; Xi, B.; Kai, S.; Zhang, J.; Feng, J.; Xiong, S. Rationally Incorporated MoS_2/SnS_2 Nanoparticles on Graphene Sheets for Lithium-Ion and Sodium-Ion Batteries. *ACS Appl. Mater. interfaces* **2017,** *9*, 27697-27706.

(S7) Wang, Y.; Zhou, J.; Wu, J.; Chen, F.; Li, P.; Han, N.; Huang, W.; Liu, Y.; Ye, H.;

Zhao, F.; Li, Y. Engineering SnS_2 Nanosheet Assemblies for Enhanced Electrochemical Lithium and Sodium Ion Storage. *J. Mater. Chem. A* **2017,** *5*, 25618-25624.

(S8) Liu, Y.; Yu, X.-Y.; Fang, Y.; Zhu, X.; Bao, J.; Zhou, X.; Lou, X. W. Confining SnS_2 Ultrathin Nanosheets in Hollow Carbon Nanostructures for Efficient Capacitive Sodium Storage. *Joule* **2018,** 2, 1-11.

(S9) Wang, X.; Li, X.; Li, Q.; Li, H.; Xu, J.; Wang, H.; Zhao, G.; Lu, L.; Lin, X.; Li, H.; Li, S. Improved Electrochemical Performance Based on Nanostructured SnS_2@CoS_2–rGO Composite Anode for Sodium-Ion Batteries. *Nano-Micro Letters* **2018,** *10*, 46.

(S10) Zhou, P.; Wang, X.; Guan, W.; Zhang, D.; Fang, L.; Jiang, Y. SnS_2 Nanowall Arrays toward High-Performance Sodium Storage. *ACS Appl. Mater. interfaces* **2017,** *9*, 6979-6987.

(S11) Huang, Y.; Zheng, Y.; Li, X.; Adams, F.; Luo, W.; Huang, Y.; Hu, L. Electrode Materials of Sodium-Ion Batteries toward Practical Application. *ACS Energy Letters* **2018**, *3*, 1604-1612.

(S12) Ren, W.; Zhu, Z.; An, Q.; Mai, L. Emerging Prototype Sodium-Ion Full Cells with Nanostructured Electrode Materials. *Small* **2017**, *13*, 1604181.